







**Strain-mediated magnetoelectricity probed by Raman spectroscopy in  $h$ -ErMnO<sub>3</sub>**A. Correa <sup>1</sup>, D. A. B. Barbosa <sup>2</sup>, A. S. de Menezes <sup>1</sup>, C. L. Valente-Rodrigues <sup>3</sup>,  
Surender Kumar Sharma <sup>4,1</sup> and C. C. Santos <sup>1,\*</sup><sup>1</sup>*Departamento de Física, Universidade Federal do Maranhão, 65080-805 São Luís, Maranhão, Brazil*<sup>2</sup>*Coordenação de Licenciatura em Ciências Naturais - Física, Universidade Federal do Maranhão, 65418-000 Bacabal, Maranhão, Brazil*<sup>3</sup>*Centro Brasileiro de Pesquisas Físicas, 22290-180 Rio de Janeiro, Rio de Janeiro, Brazil*<sup>4</sup>*Department of Physics, Central University of Punjab, 151 401 Bathinda, India*

(Received 12 December 2022; revised 24 May 2023; accepted 8 June 2023; published 5 July 2023)

We show the role of strain in magnetoelectric effect through coupling between order parameters and their interplay using infrared/Raman-active optical phonons in hexagonal manganite ( $h$ -ErMnO<sub>3</sub>). The magnetoelectric coupling is arbitrated through strain from infrared-active phonons, which by symmetry are also Raman active. The identification of the primitive order parameters by spin-phonon coupling opens a promising avenue to realize the strategy based on coupling of spins, optical phonons, and strain to create magnetoelectrics with strain-mediated interaction through spin-lattice coupling in bulk inducing a ferromagnetic-ferroelectric state in an antiferromagnetic-paraelectric phase.

DOI: [10.1103/PhysRevB.108.014101](https://doi.org/10.1103/PhysRevB.108.014101)

Multiferroics materials present at least two ferroic orders namely ferroelectricity, ferromagnetism, ferroelasticity, antiferromagnetism, and ferrotoroidicity in the same phase [1]. Magnetoelectrics are multiferroics in which ferroelectricity and ferromagnetism are coupled directly or indirectly via strain and the change in electrical properties occur by magnetic fields or vice versa. The coupling coefficient of directly coupled magnetoelectrics is linear with electric or magnetic fields. For indirect coupling, cross terms are proportional to strain with quadratic dependence on electric and magnetic fields [2]. Such possibility motivated the elaboration of a strategy to create magnetoelectrics with strain-mediated interaction of ferroelectricity and antiferromagnetism using a strong coupling of strain and infrared (IR) active phonons in an antiferromagnetic-paraelectric bulk phase especially proposed to thin films engineering [3] since ferroelectric and antiferromagnetic domains are coincident in these materials [4]. The realization of this proposition showed that spin-phonon coupling opens a promising avenue to investigate the coupled order parameters via their wavenumber dependencies on temperature [5].

Recently, Giraldo *et al.* [6] showed that  $h$ -ErMnO<sub>3</sub> has strong magnetoelectric coupling in bulk despite the absence of a linear magnetoelectric effect. Also, Skjærvo *et al.* [7] reported a meticulous neutron diffraction investigation of the atomic structure from room temperature to 1273 K, describing local structure and order parameters for YMnO<sub>3</sub>, which is an isostructural manganite. According to this work, the atomic displacements related to the order parameter that governs the magnetoelectric coupling in hexagonal perovskites are (i) bipyramidal tilting in the  $c$  axis (O1-Mn-O2 angle), (ii) bipyramidal tilting in the  $ab$  plane (O3-Mn-O4 angle), and (iii) off-centering displacement of the rare-earth ion [7]. Then, fer-

roelectric order in  $h$ -ErMnO<sub>3</sub> is related to dislocation of the Er ion in the  $c$  axis, and the antiferromagnetic order is connected to both angles. Further, very recent density functional theory (DFT) calculations suggested that manganese and oxygen displacements at the  $ab$  plane of the MnO<sub>5</sub> breathing mode in ErMnO<sub>3</sub> can be used to control magnetic order [8].

As mentioned before, only IR-active phonons contribute to magnetoelectricity. However, for  $h$ -ErMnO<sub>3</sub>, all infrared phonons are also Raman active. Therefore, we applied Raman spectroscopy to investigate the atomic displacements related to order parameters responsible for magnetoelectric coupling at low temperatures in  $h$ -ErMnO<sub>3</sub>. A detailed synthesis and characterization procedure is given in Ref. [9]. The influence of negative expansion of the  $c$  axis and the magnetostriction is also investigated. The displacements of the ions related to the order parameters are connected with the 118-, 298-, and 686-cm<sup>-1</sup> modes in Raman spectra. These phonon wavenumbers showed an intricate dependence on temperature due to several concurrent mechanisms. The 232-cm<sup>-1</sup> mode showed a clear quadratic wavenumber dependence with temperature over the entire range of a primary order parameter.

In this paper, we used temperature-dependent Raman spectroscopy to investigate local structural features in  $h$ -ErMnO<sub>3</sub>. The ErMnO<sub>3</sub> hexagonal structure with space group  $P6_3cm$  has 23 IR-active modes that are also Raman active due to its noncentrosymmetric symmetry. Thus,  $h$ -ErMnO<sub>3</sub> has a total of 38 Raman-active modes distributed as  $\Gamma_{\text{Raman}} = 9A_1 \oplus 15E_2 \oplus 14E_1$  being the IR-active modes represented by  $\Gamma_{\text{IR}} = 9A_1 \oplus 14E_1$ . The Raman spectrum at 300 K for  $h$ -ErMnO<sub>3</sub> is typical for hexagonal perovskites [10,11] and shows, in general, 14 bands (see Fig. S4 and Table S2 of the Supplemental Material [9]). We selected and analyzed six bands in more detail, whose classification and atomic movements are described in Table I. A comparison between these six selected phonons in  $h$ -ErMnO<sub>3</sub> and a single crystal

\*Corresponding author: [clenilton.cs@ufma.br](mailto:clenilton.cs@ufma.br)

TABLE I. Selected Raman mode assignments and wavenumbers for *h*-ErMnO<sub>3</sub>.

| $\omega$ (cm <sup>-1</sup> ) present work @ 300 K | $\omega$ (cm <sup>-1</sup> ) single crystal @ 300 K | Assignments | Atomic displacements                            |
|---|---|-------------|---|
| 686   | 684   | $A_1$       | $+z(\text{O1}) - z(\text{O2})$                  |
| 464   | 464   | $A_1$       | $+x, y(\text{O1}, \text{O2}) - x, y(\text{Mn})$ |
| 298   | 297   | $E_2$       | $z(\text{O2}, \text{O1}), x, y(\text{O4})$      |
| 232   | 234   | $E_2$       | $+x, y(\text{Mn}) - x, y(\text{O3}, \text{O4})$ |
| 139   | 138   | $E_2$       | $+x, y(\text{Er1}) - x, y(\text{Er2})$          |
| 118   | 123   | $A_1$       | $+z(\text{Er1}) - z(\text{Er2})$                |

is also presented [12]. These phonons are associated with the atomic displacements related to the order parameters in *h* manganites [7]. The  $A_1$  (686) mode corresponds to stretching vibrations of the apical oxygens O1 and O2 in the manganese tetragonal bipyramids. The  $A_1$  (464) mode corresponds to in-phase stretching vibrations of apical oxygens O1 and O2 in the manganese tetragonal bipyramids and relative out-of-phase displacement of Mn ions in the plane. The  $E_2$  (298) mode corresponds to the lattice mode involving displacements of O<sup>2-</sup> and Mn<sup>3+</sup> ions and depends on Mn-O-Mn distance and its force constant. The  $E_2$  (232) mode involves Mn in-phase and O out-of-phase atomic displacements in the plane and reflects the Er dependence of Mn-O bond lengths and their force constants [12]. The  $E_2$  (138) mode corresponds to out-of-phase displacements of the Er<sup>3+</sup> rare-earth ion along the *xy* plane. While the  $A_1$  (118) mode corresponds to Er<sup>3+</sup> rare-earth ion displacements along *z* direction, it is essential to notice that 118-cm<sup>-1</sup> mode has atomic displacements related to the formation of electric dipoles at *h*-ErMnO<sub>3</sub> [6].

The temperature-dependent phonon spectra of *h*-ErMnO<sub>3</sub>, collected from 10 to 220 K, are shown in Fig. S5 in the Supplemental Material [9]. No Raman spectra were collected between 230 and 290 K due to the intense laser annealing effect on the sample—intensified by high-vacuum conditions in the cryostat sample compartment, even lowering the laser power (<0.1 mW). The spectra showed the same typical behavior of hexagonal *P6<sub>3</sub>cm* structures exhibiting four main bands up to room temperature. No space group change or symmetry breaking, such as appearing, vanishing, or splitting of phonons, is observed in temperature-dependent Raman spectra. Contrarily, a magnetic phase transition can be observed for other manganites of this simple-perovskite family [13]. We obtained the wavenumber dependence with temperature for the optical phonons from the recursive adjustments of the Raman spectra, as shown in Fig. 1. A comparison of our data with the temperature-dependent variation of wavenumbers obtained for the single crystal is provided in Fig. S6 in Ref. [9].

Generally, in the absence of significant structural changes, we expect a reduction in the unit cell volume due to atomic approximations allowed by lower vibration caused by the decrease in the temperature. Contrarily, the phonon wavenumber (linewidth) is expected to increase (decrease) since the atomic approximations will intensify their interactions, thus the related vibrational mode stiffens. The model proposed by Balkanski [14] for wavenumber dependence on temperature accounts for the anharmonic contribution to

phonon wavenumber as follows:

$$\omega = \omega_0 - \lambda \left[ 1 + \frac{2}{e^{\hbar\omega_0/2k_B T} - 1} \right], \quad (1)$$

where  $\lambda$  and  $\omega_0$  are the coupling constant and the phonon frequency at 0 K; both are adjustable parameters of the experimental curve. In that manner, in the absence of structural transition or any other anomaly, the phonon wavenumber usually increases monotonically and exhibits saturation for

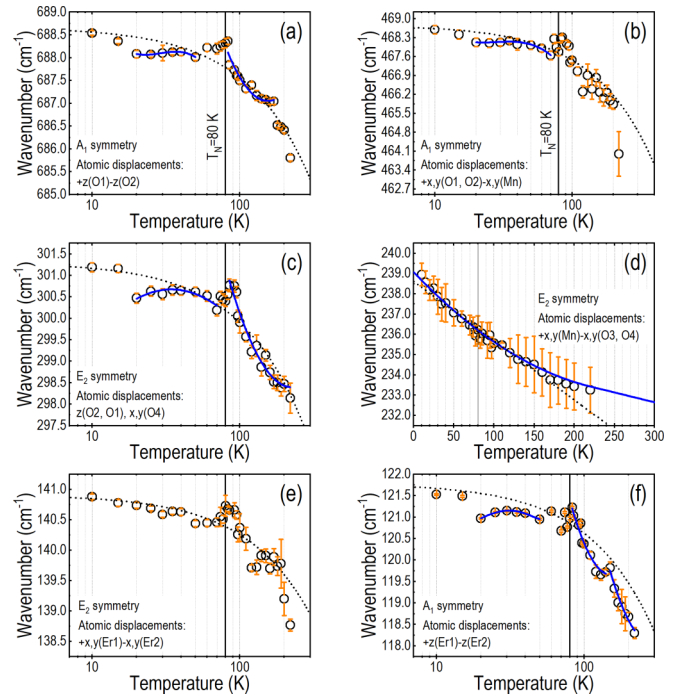


FIG. 1. Wavenumber versus temperature for  $A_1$  mode (686 cm<sup>-1</sup>): symmetrical stretching of Mn against O (a),  $A_1$  mode (464 cm<sup>-1</sup>): symmetrical stretching of Mn against O (b),  $E_2$  lattice mode (298 cm<sup>-1</sup>): antisymmetric displacement of Mn against O (c), and also the  $E_2$  lattice modes (232 cm<sup>-1</sup>) (d), the  $A_1$  mode (138 cm<sup>-1</sup>): Er in *xy* plane (e) and  $A_1$  mode (118 cm<sup>-1</sup>): Er in *z* direction (f) for *h*-ErMnO<sub>3</sub>. The vertical solid line at 80 K represents the paramagnetic-antiferromagnetic transition temperature ( $T_N$ ). The dashed black lines are the mathematic fit based on the Balkanski model, and the solid blue lines are the quadratic fit for the modes that couple the antiferromagnetic and ferroelectric order parameters. The linear scale is used in (d) to emphasize the difference between the Balkanski model and the quadratic correlation (solid blue line) between wavenumber and temperature.

a specific temperature range at low temperatures. Using this background, we can apply Raman spectroscopy to analyze, at the local scale, the connection between deviations in monotonic behavior of the phonon's wavenumber with possible magnetic transitions and the coupling of magnetic, structural, and polar order.

Our magnetic data showed that the antiferromagnetic moments dominate the magnetic regime at a local scale above 200 K in  $h$ -ErMnO<sub>3</sub> (Fig. S7 in the Supplemental Material [9]). Below 200 K, the paramagnetic moments due to Er<sup>3+</sup> ions strongly influence the Mn<sup>3+</sup> antiferromagnetic moments. At the same time, inspecting the bulk properties,  $h$ -ErMnO<sub>3</sub> presents a clear magnetic transition from paramagnetic to antiferromagnetic phase at 80 K. Therefore, on cooling, we expect to observe the characteristic stiffening of the modes due to the approximation of orbitals with opposite spins as observed for single crystals [12]. This magnetic transition is attributed to the antiferromagnetic ordering of the Mn spins in the Mn<sup>3+</sup>-O<sup>2-</sup>-Mn<sup>3+</sup> bond, while the Er<sup>3+</sup> magnetic moments remain paramagnetic. Thus, modifications at the bond's elastic constant due to magnetic ordering will be detected in the phonons if the ions have enough magnetic moments at their sublattices. We know so far that the magnetic moments of Er (9.6  $\mu_B$ ) and Mn (4.9  $\mu_B$ ) [15] in  $h$ -ErMnO<sub>3</sub> are locally activated at different temperatures [16]. However, the dynamics observed by analyzing the vibrational modes of the Mn and Er sublattices are more complex. The stiffening of the modes related to each sublattice starts at different temperatures and does not follow the Balkanski model [14]. Also, unexpected phonon softenings at the investigated temperature range show the coupling in the different sublattices.

In Fig. 1, we show the wavenumber temperature dependence of the selected modes. The observed modes reveal several features that deviate from the usual anharmonic behavior. The 686-cm<sup>-1</sup> mode corresponds to the symmetric stretching of the MnO<sub>5</sub> molecular groups [12], and is sensitive to possible changes in the magnetic ordering and displacements suffered at the metallic cations as the system is cooled. We observed a sharp increase in wavenumber for all modes on cooling. Contrary to what was observed in single crystals [12], the 686-cm<sup>-1</sup> mode presents a deviation from the monotonic behavior from 170 K that extends to the Néel temperature (80 K), characterized by the quadratic profile of the phonon wavenumber. The stiffening of the 686-cm<sup>-1</sup> mode around 80 K is expected due to the antiferromagnetic ordering of the Mn sublattice resulting in its known magnetic transition. However, unlike in single crystals [12], the deviation from the usual anharmonic behavior for the vibrational modes shows that Mn spins influence phonon behavior at much higher temperatures than expected, around 170 K. Observing the lattice parameters (Fig. S8 [9]), we verified that the strain dependence with temperature matches the profile of the vibrational mode in the interval, evidencing the coupling between strain and magnetic ordering in  $h$ -ErMnO<sub>3</sub>. Furthermore, some peculiarities still appear in this temperature interval: the mode softens almost monotonously down to 60 K; below that, another softening between 50 and 20 K, and after that, the mode stiffens to the expected anharmonic tendency. Surprisingly, softening around 50 K occurs in the region where magnetoelectric coupling is reported [17].

Also, comparing all the modes, we observed the same softening in modes that involve Mn and O displacements and the Er displacement in the  $c$  axis. The most sensitive modes are the antisymmetric stretching (298 cm<sup>-1</sup>) relative to Mn-O displacements in the equatorial plane ( $x, y$ [O<sub>4</sub>]) and in the apical plane ( $z$ [O<sub>1</sub>, O<sub>2</sub>]) and the Er lattice mode (118 cm<sup>-1</sup>). Due to increasing interaction between the Mn spin moments, which tend to order antiferromagnetically as the temperature decreases, the antisymmetric stretching mode at 298 cm<sup>-1</sup> is notably more sensitive to the magnetostriction effect and reflects the excellent correlation between 686- and 118-cm<sup>-1</sup> modes. The 298- and 118-cm<sup>-1</sup> modes start to couple magnetically around 200 K but with two different onsets. Both follow quadratic dependence with temperature from 200 to 80 K, while the 118-cm<sup>-1</sup> mode presents two regimes: one from 200 to 150 K and another from 150 to 80 K.

The existence of two different regimes in the spin-lattice coupling in  $h$ -ErMnO<sub>3</sub>, evidenced by the wavenumber dependence with the temperature of the Er lattice mode (118 cm<sup>-1</sup>), shows the activation of the Er paramagnetic moments at the ferroelectric sublattice. Also, the temperature of Er paramagnetic moment activation reflects in a gradual linear stiffening between 150 and 220 K of the 686-cm<sup>-1</sup> phonon, which is susceptible to magnetic ordering. Below 150 K, both modes (118 and 686 cm<sup>-1</sup>) keep quadratically stiffening until  $T_N$ . Below  $T_N$ , some small phonon softenings are observed via resonant ultrasound spectroscopy (RUS) [18]. The renormalization of the phonon frequency with a linear profile in the Mn sublattice indicates a special case of order parameter coupling, assigned to more restricted magnetic symmetries and the possibility of linear magnetoelectric coupling [19]. Still, the linear profile of the softening of the Mn sublattice phonon at this temperature confirms the proposal of Meier *et al.* [16] for the interaction of Mn and Er sublattices just below  $T_N$ . Further, the anharmonic behavior is followed in the range 70–45 K. Below 45 K, we observe a new softening of the 118-cm<sup>-1</sup> mode, which coincides with the 686-cm<sup>-1</sup> mode softening. The softening below 50 K in both modes coincides with a peak in the magnetoelectric signal at 44 K [17] and is evidence of transitory ferrimagnetic alignments between Er and Mn atomic layers down to 20 K. Below 20 K, the phonons stiffen due to spin flips caused by magnetic frustration and the spins realigns antiferromagnetically down to 10 K.

Raman spectroscopy relates these order parameters  $Q$  with variations in phonon linewidth ( $\Delta\Gamma$ ) and square of frequency ( $\Delta\omega^2$ ):

$$\Delta\Gamma \propto \Delta\omega^2 \propto AQ^2 + BQ^4, \quad (2)$$

where  $\Gamma$  is the phonon linewidth,  $\omega$  is the phonon wavenumber,  $Q$  is the order parameter,  $A$  and  $B$  are the coupling constants for quadratic and fourth-order parameters, respectively, with  $B$  generally small. Also, if  $\Delta\omega$  is small (<2%),  $\Delta\omega^2$  can be approximated by  $\Delta\omega^2 \sim \Delta\omega$  [20–22]. On the other hand, the spin-lattice coupling proposed by Fennie *et al.* [3] uses an IR-active mode to couple ferromagnetism and ferroelectricity in the same phase creating a strong ferromagnetic-ferroelectric state which uses strain to tune the multiple-order parameters. This spin-phonon coupling mechanism was used to create a strong ferromagnetic-ferroelectric



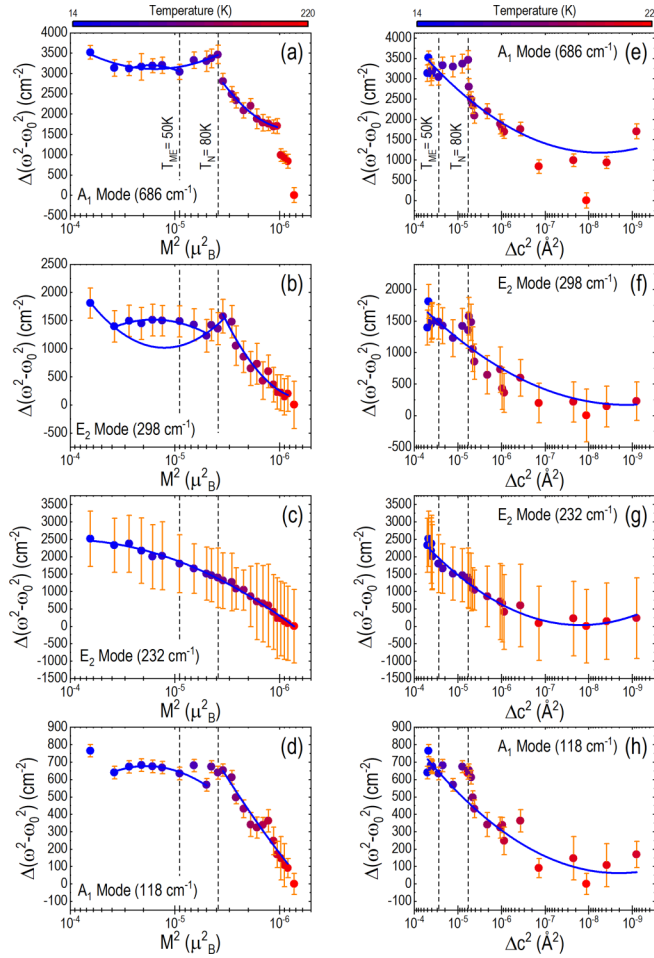


FIG. 2. Dependence of the squared position differences of  $A_1$  mode (686),  $E_2$  mode (298),  $E_2$  mode (232), and  $A_1$  mode (118) on the magnetization square (a)–(d) and strain square (e)–(h), respectively. The vertical dashed black lines indicate  $T_N$  (80 K) and  $T_{ME}$  (50 K). The solid blue lines are the quadratic fits. The modes  $E_2$  are also IR active: 298  $\text{cm}^{-1}$  mode is assigned to the antisymmetric displacement of the O4 in  $xy$  plane and the O2 and O1 in apical positions against Mn, while 232  $\text{cm}^{-1}$  mode is assigned to the antisymmetric displacement of O3 and O4 against Mn in  $xy$  plane.

state in  $\text{EuTiO}_3$  thin films [5] and to propose the bulk magnetoelectricity in manganites and ferrites [23]. This general spin-phonon mechanism is given as

$$\omega^2 = \omega_0^2 - \lambda \langle S_i \cdot S_j \rangle, \quad (3)$$

where  $\omega$  is the wavenumber of the IR-active phonon,  $\omega_0$  is the phonon frequency at 0 K,  $\lambda$  is the coupling constant, and  $\langle S_i \cdot S_j \rangle$  is the correlation spin function between the nearest neighbor spins. Thus, the temperature dependence of the wavenumber carries the magnetization and strain response of multiple order parameters for  $h\text{-ErMnO}_3$  and can be squared separately with magnetization and strain to obtain the coupling constant profile and sign.

Figure 2 shows the dependence with the strain and magnetization squares of the difference on the wavenumber squares. We can observe the quadratic coupling constants convolution present at each mode. The most notable coupling constants are related to the IR-active  $E_2$  (232) mode and reflect the

pure quadratic dependence of the  $\Delta\omega^2$  with magnetic and elastic orders. Looking back on the temperature dependence of the wavenumber for the  $E_2$  (232) mode over the entire temperature range [Fig. 1(d)], one would presume a pure  $-\lambda^2$  coupling constant as the primitive order parameter. Surprisingly, Figs. 2(c)–2(g) show coupling constants for the  $E_2$  (232) mode that differ in the sign for magnetic and elastic orders. For the entire magnetic dependence, the coupling constant is of the form  $-\lambda^2$ , while for the strain dependence, the coupling constant shows a  $\lambda^2$  profile. Also, the  $E_2$  (232) mode corresponds to ion displacements related to the  $K_3$  crystallographic mode, thus representing a primitive order parameter [8].

Once the 232- $\text{cm}^{-1}$  mode has  $E_2$  symmetry and does not account for linear magnetoelectric coupling [23], the alternative way to couple magnetic and electric order is via strain, as we can see from the inset in Fig. S8e [9]. Besides the linear magnetoelectricity being symmetry forbidden for  $h\text{-ErMnO}_3$  [6], the formation of boundaries, due to the polycrystalline character of the sample, enhance the interface interactions. The grain boundaries are interfaces where we find the coexistence of antiferromagnetic and ferroelectric domains at the same position [24], which couple strain to magnetic order. This coupling permits the existence of high-order symmetry terms,  $\lambda^2 eM$  and  $-\lambda^2 e^2 M^2$ , in hexagonal symmetry [18,25]. As the polar order parameter is essentially a lattice distortion on the Er-O polygons, ferroelectric order is fundamentally coupled to strain, which makes it possible to control the magnetoelectric coupling in polycrystalline  $h\text{-ErMnO}_3$  through lattice strain.

The  $E_2$  (232) mode shows that the equatorial bonds of Mn-O3 and Mn-O4 govern the coupling between elastic and magnetic order. The relative displacements of the Mn and the oxygen atoms O3 and O4 in the  $xy$  plane are directly coupled to the magnetic order in the  $z$  axis through the O1-Mn-O2 bridge and the ferroelectric order through Er-O3 and Er-O4 bonds. The magnetostriction, generated from frustration due to  $\text{Mn}^{3+}$  spins' short-range magnetic interaction, links to the  $\text{Er}^{3+}$  polar order via ferroelectric-antiferromagnetic coupling driven by the equatorial oxygens, thus allowing us to engineer different properties and ground states on single-phase polycrystalline  $h\text{-ErMnO}_3$  [26]. Observing the behavior of the other modes in Fig. 2, we found that the  $E_2$  (298) IR-active mode shows an excellent correlation with the coupling constants of the  $A_1$  (686) and  $A_1$  (118) Raman-active modes. The general behavior of the coupling constant is the same for the 686-, 298-, and 118- $\text{cm}^{-1}$  modes and displays a competition between magnetic and elastic orders. There is a clear convolution of the coupling constants originated by the magnetic and elastic orders that reflect in the concavity of the  $\Delta\omega^2$  curve with each parameter.

From 200 K down to  $T_N$ , these modes reflect the same  $\lambda^2$  coupling constant due to strong strain in the lattice originating in the magnetostriction due to  $\text{Mn}^{3+}$  antiferromagnetic spins dominating short-range magnetic interaction at high temperatures. Below  $T_N$ , the coupling constants between the  $A_1$  (686) and  $A_1$  (118) modes assume the same form ( $\lambda^2$ ), and the lattice frustration plays an important role in modulating the interplanar magnetic alignment of  $\text{Mn}^{3+}$  ions. At  $T = 50$  K, this alignment becomes ferrimagnetic, as shown by the softening trend of the  $A_1$  (686) mode. Additionally, the

relative displacements between Mn and the O atoms in the  $xy$  plane and  $z$  axis in the  $E_2$  (298) mode correspond to the  $K_1$  crystallographic mode as investigated by Tošić *et al.* [8] via DFT. The  $K_1$  mode has a quadratic coupling to the  $\text{ErMnO}_3$  magnetization, as shown in Fig. 2(b).

The magnetostriction mode,  $E_2$  (298), couples the atomic vibrations of the  $\text{MnO}_5$  blocks, the  $A_1$  (686) mode, with the strain along the  $c$  axis (Er atoms), and this coupling extends down to low temperatures. Hence, the ferroelectric mode,  $A_1$  (118), which corresponds to the formation of electric dipoles at the Er site, couples to magnetization via strain to generate the magnetoelectric effect in the polycrystalline bulk around 50 K. Strikingly in the 25–50-K interval, the  $A_1$  (686) mode presents a change in the general trend of the coupling constant. Below 50 K, the coupling constant changes from  $+\lambda^2$  to  $-\lambda^2$ , and the  $A_1$  (686) mode starts to couple to the  $A_1$  (118) mode through the  $E_2$  (298) mode [see the solid blue line in Figs. 2(b) and 2(f)]. The existence of these quadratic couplings for magnetic and elastic orders permits the occurrence of the crossed bilinear magnetoelectric coupling for the single phase  $h$ - $\text{ErMnO}_3$  when the magnetic structure achieves the ferrimagnetic ordering at the magnetoelectric transition temperature (50 K) [18].

Thus, the magnetoelectric coupling becomes mediated by the  $E_2$  (298) mode because it links the magnetism at the  $xy$  plane and the strain at the  $z$  axis due to the O1, O2, and O4 ion displacements relative to Mn. The strain mediation of the magnetoelectric coupling in the polycrystalline  $h$ - $\text{ErMnO}_3$  is possible since ferroelectric domains always coincide with antiferromagnetic domains [4].

An alternative way of investigating the coupling of phonons with the elastic and magnetic ordering is to observe the dependence of the phonon linewidth on these parameters. Figure 3 shows the phonon linewidth dependence with linear strain and squared magnetization. The energies of 118-, 232-, and 686- $\text{cm}^{-1}$  phonons vary after the magnetic transition below 80 K and below 50 K in the magnetoelectric coupling. Interestingly, the 686- $\text{cm}^{-1}$  mode energy decreases from 50 to 80 K for both magnetic and strain increase, while the 118- $\text{cm}^{-1}$  mode energy increases with the magnetization and strain at the same interval indicating the coupling of both phonons for the magnetoelectric effect. Below 50 K, the energies of the 686- and 118- $\text{cm}^{-1}$  modes decrease with increasing magnetization, while, for the 232- $\text{cm}^{-1}$  mode, the energy decreases with strain and magnetization just below the Néel temperature, persisting until  $T = 25$  K. On the other hand, the energy of the 298- $\text{cm}^{-1}$  mode remains stable to both magnetization and strain variations over the entire range indicating the 298- $\text{cm}^{-1}$  mode acts like a bridge to transmit the energy from the 232- $\text{cm}^{-1}$  mode vibration to the other phonons. Further, we noticed the wavenumber dependence with magnetization and strain of the order parameters and symmetry considerations also allow the existence of fourth order coupling ( $BQ^4$  term), which suggests the existence of the piezomagnetolectric effect [27] in polycrystalline  $h$ - $\text{ErMnO}_3$  (see Fig. S9 [9]).

In summary, we demonstrated the coupling between multiple order parameters and their interplay with the magnetoelectric effect in  $h$ - $\text{ErMnO}_3$ . A high magnetostriction response is demonstrated through the Einstein-Grüneisen

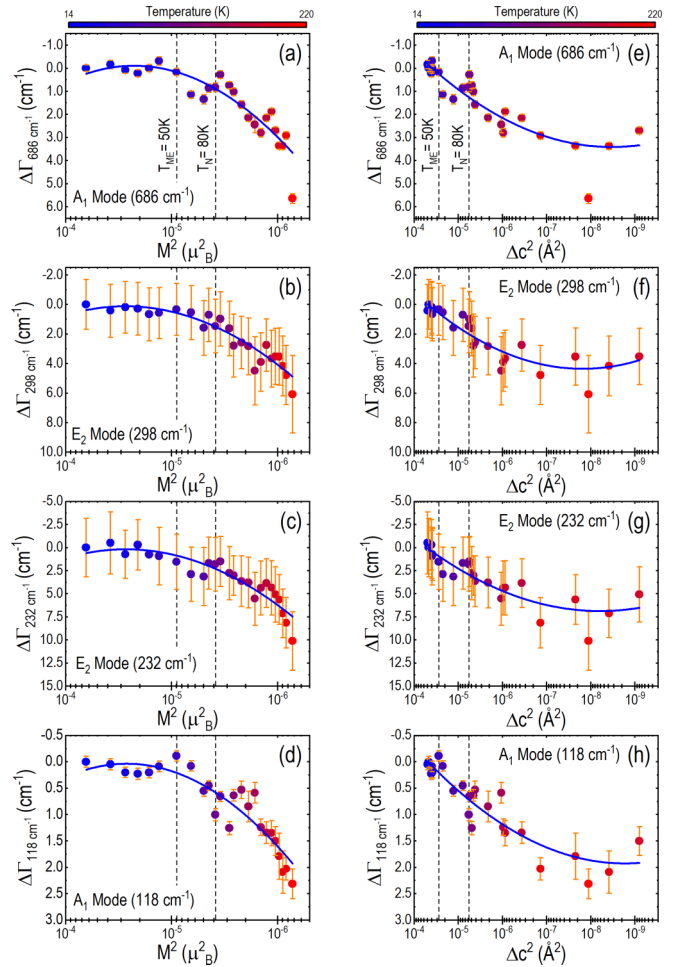


FIG. 3. Dependence of the linewidth of  $A_1$  mode (686),  $E_2$  mode (298),  $E_2$  mode (232), and  $A_1$  mode (118) on the magnetization square (a)–(d) and strain square (e)–(h), respectively. The vertical dashed black lines indicate  $T_N$  (80 K) and  $T_{ME}$  (50 K). The solid blue lines are the quadratic fits, and the shaded grey area is the magnetoelectric region.

model. The magnetic analysis revealed the local antiferromagnetism at high temperatures due to  $\text{Mn}^{3+}$  spins, while the Er paramagnetic moments are activated at a local scale  $\sim 200$  K and influenced the local magnetic ordering down to 10 K. Raman spectroscopy probed the ions' displacements connected to the order parameters related to the modes at 118, 298, and 686  $\text{cm}^{-1}$  and detected the spin-lattice coupling in Mn and Er sublattices with no evidence of symmetry breaking. These modes showed an intricate wavenumber dependence on temperature due to several concurrent mechanisms at low temperatures. Contrarily, the 232- $\text{cm}^{-1}$  mode showed a clear quadratic wavenumber dependence on temperature, a primary order parameter coupled to strain and magnetization.

The authors are grateful to Conselho Nacional de Desenvolvimento Científico e Tecnológico–CNPq (Grant No. PQ-305806/2020-3), Coordenação de Aperfeiçoamento Pessoal de Nível Superior–CAPES (Finance Code 001), and Fundação de Amparo à Pesquisa e ao Desenvolvimento Científico e Tecnológico do Maranhão–FAPEMA (Grants

No. UNIVERSAL-01064/2019, No. INFRA-02050/21, and No. INFRA-02203/21) for financial support. A.C. acknowledges the scholarship from FAPEMA (BD-01477/19), and D.A.B.B. acknowledges the Universidade Federal do Maranhão (UFMA) for institutional support (PVBAC866-2017).

Authors contributed as follows: conceptualization: D.A.B.B. and C.C.S.; methodology: A.C., A.S.d.M., C.L.V.-R., and C.C.S.; validation: all authors; formal analysis:

all authors; investigation: D.A.B.B., A.S.d.M., S.K.S., and C.C.S.; resources: A.C., D.A.B.B., A.S.d.M., S.K.S., and C.C.S.; writing, original draft preparation: A.C., D.A.B.B., and C.C.S.; writing, review and editing: D.A.B.B., A.S.d.M., S.K.S., and C.C.S.; supervision: D.A.B.B. and C.C.S.; project administration: C.C.S.; funding acquisition: A.S.d.M. and C.C.S. All authors have read and agreed to the published version of the manuscript.

- [1] N. A. Spaldin and R. Ramesh, Advances in magnetoelectric multiferroics, *Nat. Mater.* **18**, 203 (2019).
- [2] W. Eerenstein, N. D. Mathur, and J. F. Scott, Multiferroic and magnetoelectric materials, *Nature (London)* **442**, 759 (2006).
- [3] C. J. Fennie and K. M. Rabe, Magnetic and Electric Phase Control in Epitaxial  $\text{EuTiO}_3$  from First Principles, *Phys. Rev. Lett.* **97**, 267602 (2006).
- [4] M. Fiebig, T. Lottermoser, D. Fröhlich, A. V. Goltsev, and R. V. Pisarev, Observation of coupled magnetic and electric domains, *Nature (London)* **419**, 818 (2002).
- [5] J. H. Lee, L. Fang, E. Vlahos, X. Ke, Y. W. Jung, L. F. Kourkoutis, J. -W. Kim, P. J. Ryan, T. Heeg, M. Roeckerath *et al.*, A strong ferroelectric ferromagnet created by means of spin–lattice coupling, *Nature (London)* **466**, 954 (2010).
- [6] M. Giraldo, Q. N. Meier, A. Bortis, D. Nowak, N. A. Spaldin, M. Fiebig, M. C. Weber, and T. Lottermoser, Magnetoelastic coupling of domains, domain walls and vortices in a multiferroic with independent magnetic and electric order, *Nat. Commun.* **12**, 3093 (2021).
- [7] S. H. Skjærvø, Q. N. Meier, M. Feyngenson, N. A. Spaldin, S. J. L. Billinge, E. S. Bozin, and S. M. Selbach, Unconventional Continuous Structural Disorder at the Order-Disorder Phase Transition in the Hexagonal Manganites, *Phys. Rev. X* **9**, 031001 (2019).
- [8] T. N. Tošić, Q. N. Meier, and N. A. Spaldin, Influence of the triangular Mn-O breathing mode on the magnetic ordering in multiferroic hexagonal manganites, *Phys. Rev. Res.* **4**, 033204 (2022).
- [9] See Supplemental Material at <http://link.aps.org/supplemental/10.1103/PhysRevB.108.014101> for details of sample preparation and structural, morphological, compositional, vibrational, and magnetic characterizations.
- [10] H. Fukumura, S. Matsui, H. Harima, K. Kisoda, T. Takahashi, T. Yoshimura, and N. Fujimura, Raman scattering studies on multiferroic  $\text{YMnO}_3$ , *J. Phys.: Condens. Matter* **19**, 365239 (2007).
- [11] M. N. Iliev, H.-G. Lee, V. N. Popov, M. V. Abrashev, A. Hamed, R. L. Meng, and C. W. Chu, Raman- and infrared-active phonons in hexagonal  $\text{YMnO}_3$ : Experiment and lattice-dynamical calculations, *Phys. Rev. B* **56**, 2488 (1997).
- [12] J. Vermette, S. Jandl, and M. M. Gospodinov, Raman study of spin–phonon coupling in  $\text{ErMnO}_3$ , *J. Phys.: Condens. Matter* **20**, 425219 (2008).
- [13] S. Lee, A. Pirogov, M. Kang, K. H. Jang, M. Yonemura, T. Kamiyama, S.-W. Cheong, F. Gozzo, N. Shin, H. Kimura *et al.*, Giant magneto-elastic coupling in multiferroic hexagonal manganites, *Nature (London)* **451**, 805 (2008).
- [14] M. Balkanski, R. F. Wallis, and E. Haro, Anharmonic effects in light scattering due to optical phonons in silicon, *Phys. Rev. B* **28**, 1928 (1983).
- [15] J. R. Sahu, A. Ghosh, A. Sundaresan, and C. N. R. Rao, Multiferroic properties of  $\text{ErMnO}_3$ , *Mater. Res. Bull.* **44**, 2123 (2009).
- [16] D. Meier, H. Ryll, K. Kiefer, B. Klemke, J.-U. Hoffmann, R. Ramesh, and M. Fiebig, Mutual induction of magnetic 3D and 4F order in multiferroic hexagonal  $\text{ErMnO}_3$ , *Phys. Rev. B* **86**, 184415 (2012).
- [17] N. Iwata and K. Kohn, Magnetoelastic effect and rare earth magnetic ordering of  $\text{ErMnO}_3$ , *Ferroelectrics* **219**, 161 (1998).
- [18] C. M. Fernandez-Posada, C. R. S. Haines, D. M. Evans, Z. Yan, E. Bourret, D. Meier, and M. A. Carpenter, Magnetoelastic properties of multiferroic hexagonal  $\text{ErMnO}_3$ , *J. Magn. Magn. Mater.* **554**, 169277 (2022).
- [19] A. P. Levanyuk and D. G. Sannikov, Improper ferroelectrics, *Sov. Phys. Usp.* **17**, 199 (1974).
- [20] E. K. H. Salje and U. Bismayer, Hard mode Spectroscopy: The concept and applications, *Phase Transit.* **63**, 1 (1997).
- [21] D. Yang, G. I. Lampronti, C. R. S. Haines, and M. A. Carpenter, Magnetoelastic coupling behavior at the ferromagnetic transition in the partially disordered double perovskite  $\text{La}_2\text{NiMnO}_6$ , *Phys. Rev. B* **100**, 014304 (2019).
- [22] E. K. H. Salje, Hard mode spectroscopy: Experimental studies of structural phase transitions, *Phase Transit.* **37**, 83 (1992).
- [23] H. Das, A. L. Wysocki, Y. Geng, W. Wu, and C. J. Fennie, Bulk magnetoelectricity in the hexagonal manganites and ferrites, *Nat. Commun.* **5**, 2998 (2014).
- [24] T. Lottermoser, T. Lonkai, U. Amann, D. Hohlwein, J. Ihringer, and M. Fiebig, Magnetic phase control by an electric field, *Nature (London)* **430**, 541 (2004).
- [25] R. I. Thomson, T. Chatterji, C. J. Howard, T. T. M. Palstra, and M. A. Carpenter, Elastic anomalies associated with structural and magnetic phase transitions in single crystal hexagonal  $\text{YMnO}_3$ , *J. Phys.: Condens. Matter* **26**, 045901 (2014).
- [26] E. Bousquet, M. Dawber, N. Stucki, C. Lichtensteiger, P. Hermet, S. Gariglio, J.-M. Triscone, and P. Ghosez, Improper ferroelectricity in perovskite oxide artificial superlattices, *Nature (London)* **452**, 732 (2008).
- [27] H. Grimmer, The piezomagnetoelastic effect, *Acta Cryst. A* **48**, 266 (1992).